

# Network-based prediction of drug combinations with quantum annealing

Diogo Ramos

*Faculdade de Ciências (FCUP), Universidade do Porto, Portugal*

Bruno Coutinho

*Institute of Communications and Navigation, German Aerospace Center (DLR), Weßling, Germany and  
Instituto de Telecomunicações (IT), Lisboa, Portugal*

Duarte Magano\*

*Faculdade de Ciências (FCUP), Universidade do Porto, Portugal and*

*21strategies GmbH, Hallbergmoos, Germany*

(Dated: December 24, 2025)

The systematic discovery of effective drug combinations is a challenging problem in modern pharmacology, driven by the combinatorial growth of potential pairings and dosage configurations. Network medicine, modeling diseases and drugs as interconnected modules of the human protein-protein interactome, has emerged as a new paradigm for understanding disease mechanisms and drug action. In this work, we propose a quantum annealing-based algorithm for identifying effective drug combinations. Underlying our approach is the biologically motivated principle of ‘Complementary Exposure’, which posits that therapeutic drug combinations target distinct yet complementary regions of a disease module. We translate this into a quadratic unconstrained binary optimisation problem. We test our method for Diabetes Mellitus, Rheumatoid Arthritis, Asthma, and Brain Neoplasms, relying on experimentally validated drug combinations for these diseases. Our simulated quantum annealing experiments reveal that low-energy configurations align with biologically plausible combinations, demonstrating the algorithm’s ability to generate novel predictions for drug combinations.

**Keywords:** quantum annealing; network medicine; drug combinations; complementary exposure

## I. INTRODUCTION

In modern medicine, therapies frequently combine multiple drugs to treat the same disease, since combination therapy has been shown to allow lower dosages and have fewer side effects [1]. With over 1,000 drugs approved by the U.S. Food and Drug Administration targeting 3,000 human diseases [2], finding the optimal drug combination is a complex process. The challenge is further amplified by the difficulty of predicting interactions among medications. Although physicians frequently rely on experience and intuition, addressing this problem ultimately requires a systematic approach. It is well established that drugs act by targeting specific proteins in our cells, but knowing which proteins each drug targets is not sufficient. Proteins operate within a complex network of interactions — the interactome — which encodes the mechanisms underlying cellular function. While the full interactome remains far from mapped, we do have partial access to one of its key subnetworks: the protein-protein interaction (PPI) network. In this network, nodes represent proteins, and edges indicate known interactions. To date, researchers have mapped over 243,000 interactions involving more than 16,000

proteins. Although it is difficult to estimate how close this is to the complete underlying network, the existing data has already yielded major insights into the inner workings of a cell. Notably, [3, 4] found that proteins associated with the same disease tend to be in the same neighbourhood of the PPI network, forming the so-called disease modules. Building on this intuition, Cheng *et al.* [5] proposed a systematic framework for predicting drug combinations. They introduced two main concepts: complementary exposure and overlapping exposure. The idea is that individual drugs are effective when they target proteins close to the corresponding disease modules, thereby maximising exposure. However, efficient drug-drug combinations require complementary action, meaning that each drug acts on a distinct subset of proteins within the module. In contrast, when multiple drugs target overlapping protein sets, the risk of side effects increases [5].

Quantum computation has already been proposed for a range of medical applications. In 2019, Grimsley *et al.* introduced a promising approach that uses quantum adaptive variational simulations of molecular interactions for drug discovery [6]. In 2021, quantum computation was also applied to the optimisation of radiotherapy treatment plans [7]. More recently, in 2023, Moutinho *et al.* studied a quantum algorithm with direct medical implications that explicitly incorporates network structure: they proposed a quantum-walk-based method to identify missing links in

---

\* Corresponding author address: duarte.magano@fc.up.pt

complex networks, with a strong emphasis on biological networks such as PPI networks [8]. Later work suggested that this approach may offer a potential polynomial or exponential speed-up, depending on the network’s structure [9, 10]. Once again using information from PPI networks, in 2025 Marques *et al.* [11] developed an algorithm for identifying potential cancer-related targets, achieving an exponential speed-up per prediction.

Quantum annealing, a quantum computing technique tailored for solving combinatorial optimisation problems, also offers a promising direction [12, 13]. Unlike classical heuristics, which can struggle in high-dimensional energy landscapes, quantum annealers leverage quantum effects such as tunnelling to explore solution spaces differently [14]. By approximately evolving the system toward low-energy states, they may find high-quality solutions more efficiently for certain problem types, though their practical advantage over classical methods remains an active area of research [15, 16]. This capability aligns with the challenges of drug combination discovery, where evaluating every possible combination of two or more drugs can become computationally prohibitive [17].

This emerging technology has been applied to a variety of state-of-the-art combinatorial and sampling problems — notably large-scale scheduling and routing [18, 19], portfolio optimisation [20, 21], energy-grid resource allocation [22] and materials design [23] — since many such tasks map naturally to Quadratic Unconstrained Binary Optimisation (QUBO) formulations and can exploit specialised annealer embeddings and architectures. In medicine, quantum annealing has been proposed for tasks that impact drug discovery and molecular design, including conformation search and generation [24, 25], peptide and protein design [26–28] and molecular docking [29]. While largely exploratory today, these directions highlight promising hybrid workflows that combine classical preprocessing, network-based models, and annealing hardware for scalable combinatorial exploration in biomedical pipelines.

In this work, we propose a novel quantum annealing-based approach to identify potential drug combinations. Our algorithm builds on the ‘Complementary Exposure’ principle of Cheng *et al.* [5]. We first express that principle as a QUBO problem suitable for implementation on current quantum annealers and then add biologically motivated constraints to better accommodate validated drug combination datasets. Finally, we discuss and demonstrate how the presented pipeline fits within the quantum annealing paradigm by employing a Simulated Quantum Annealing (SQA) sampler to extract meaningful drug-combination predictions.

We test our approach against Diabetes Mellitus, Rheumatoid Arthritis, Asthma, and Brain Neoplasms, and their respective validated drug combinations, discussing the algorithm’s broader applicability in medicine. Our framework can generate recommendations for biologically plausible drug combinations, which

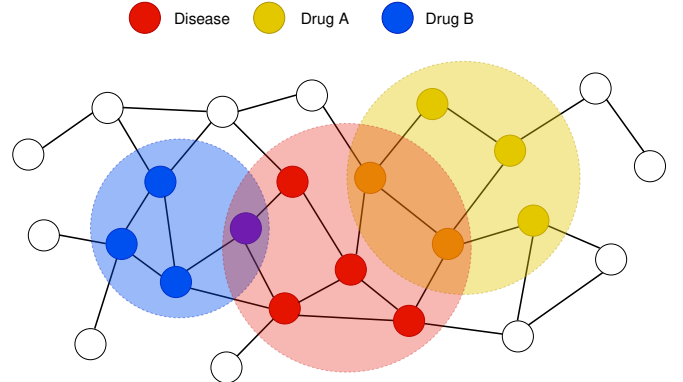


**Fig. 1: Schematic of the ‘Complementary Exposure’ principle.** Two drugs, A (yellow) and B (blue), represented by their protein targets, exhibit shared nodes with the disease module (red) in the human protein-protein interactome graph. Both drug node sets target distinct, non-overlapping regions of the disease module (red). This leads to effective perturbation of the disease-associated network neighborhood as quantified by the network proximity measures  $s_{AB} \geq 0$  and  $z_A, z_B < 0$ .

may serve as prioritized candidates for subsequent experimental validation.

## II. NETWORK PROXIMITY MEASURES

We represent molecular interactions using the human protein–protein interactome. This is an undirected graph  $\mathcal{G} = (V, E)$ , where nodes  $v \in V$  correspond to proteins and edges  $(u, v) \in E$  designate experimentally supported physical interactions. The network distances refer to shortest-path lengths on  $\mathcal{G}$ . Disease modules are defined as sets of disease-associated proteins  $Y \subset V$ , while a drug  $X$  is represented by the set of its known target proteins  $X \subset V$ .

The ‘Complementary Exposure’ principle assumes that the therapeutic value of a drug combination depends on its ability to perturb the disease-associated network neighbourhood (the disease module) in a complementary manner, while avoiding redundant targeting or excessive overlap that can increase toxicity. A diagrammatic illustration of this relationship for a drug-drug-disease combination is provided in Figure 1. Furthermore, Cheng *et al.* [5] proposes that network-based proximity can be used as a proxy to infer both the impact of a drug on a disease module and the extent of overlap between drugs. Namely, drug targets and disease modules within the human protein-protein interactome. Here, we refer to the two network-based metrics central to the ‘Complementary Exposure’ principle — *z-score* [30] and the *separation measure* [31].

The *z-score* evaluates the network-based proximity between a drug  $X$  and a disease module  $Y$ . It is defined as

$$z(X, Y) = \frac{d(X, Y) - \mu_{(X, Y)}}{\sigma_{(X, Y)}} \quad (1)$$

where  $\mu_{(X, Y)}$  and  $\sigma_{(X, Y)}$  represent the mean and standard deviation of distances from a null model. This model consists of an ensemble of degree-matched random node sets, which controls for degree-related topological biases [30, 31]. The distance  $d(X, Y)$  between a set of drug targets  $X$  and a set of disease proteins  $Y$  is defined as the average shortest-path length from each disease protein  $y \in Y$  to its nearest drug target  $x \in X$ :

$$d(X, Y) = \frac{1}{\|Y\|} \sum_{y \in Y} \min_{x \in X} d(x, y) \quad (2)$$

A negative *z-score* indicates that drug targets are closer to the disease module than expected by chance, suggesting therapeutic relevance [30]. Therefore, we give preference to disease-drug pairs with negative *z*-scores. This choice is consistent with the hypothesis that effective drugs localize near disease modules, as disease-associated genes cluster in interconnected neighborhoods [31].

While the *z-score* identifies drug-disease relationships and has been used to successfully predict monotherapies [30], its utility diminishes for combinations due to small drug-target sets and non-Gaussian randomization biases [5]. This phenomena is addressed by the *separation measure* [31]:

$$s(A, B) = \langle d_{AB} \rangle - \frac{\langle d_{AA} \rangle + \langle d_{BB} \rangle}{2} \quad (3)$$

where  $\langle d_{AB} \rangle$  is the mean shortest path between targets of drugs  $A$  and  $B$ , while  $\langle d_{AA} \rangle$  and  $\langle d_{BB} \rangle$  are the mean shortest distances of the targets of each drug individually. If a protein is a target of both sets, it has distance zero by definition. The separation measure  $s_{AB}$  serves as a topological indicator of drug interaction mechanisms. A negative value  $s_{AB} < 0$  indicates overlapping drug targets within shared network neighborhoods. Conversely, a non-negative value  $s_{AB} \geq 0$  indicates target localization in distinct topological regions, potentially leading to complementary therapeutic effects. Therefore, according to the ‘Complementary Exposure’ principle, effective drug combination must satisfy two criteria: (i) its drugs exhibit significant proximity to the disease module, as evidenced by  $z_{\text{drug A}} < 0$  and  $z_{\text{drug B}} < 0$ ; and (ii) their targets occupy disjoint regions of the interactome, quantified by  $s_{AB} \geq 0$ . These criteria ensure that combinations simultaneously maximize disease module perturbation while minimizing redundant target engagement, a hallmark of clinically viable complementary therapies [5].

Previous studies have supported these concepts by successfully predicting therapeutic drug combinations

using models based on network-derived metrics [32–34], with experimental validation reported in at least one case [34].

### III. QUANTUM ANNEALING

Quantum annealing (QA) is a quantum computing paradigm specially suited for solving combinatorial optimisation problems [13]. In QA a spin system evolves under a time-dependent Hamiltonian  $H(t)$  [35],

$$H(t) = \left(1 - \frac{t}{T}\right) H_0 + \frac{t}{T} H_p. \quad (4)$$

QA carries a transition between an initial Hamiltonian  $H_0$  at time  $t = 0$  and the *problem* Hamiltonian at time  $t = T$ . A typical choice for the initial Hamiltonian is

$$H_0 = - \sum_i \sigma_i^x,$$

since the ground state, a uniform superposition of all states in the computational basis, is simple to prepare in most platforms. The problem Hamiltonian,

$$H_p = \sum_i h_i \sigma_i^z + \sum_{i < j} J_{ij} \sigma_i^z \sigma_j^z, \quad (5)$$

encodes the cost function of the underlying optimisation problem such that its solution is found in the ground state of  $H_p$ .

The quantum adiabatic theorem ensures that, if the transition is slow enough (*i.e.*, if  $T$  is large enough), the system remains in the instantaneous ground state of  $H(t)$  throughout the entire evolution [12]. It is typically stated as follows. Let  $E_i(t)$  ( $|E_i(t)\rangle$ ) is the  $i$ -th instantaneous eigenenergy (eigenstate) of  $H(t)$ ; if the system is initialized in the ground state  $|E_0(0)\rangle$  of  $H_0$ , it will remain (approximately) in the instantaneous ground state of  $H(t)$  for all time if the following condition is satisfied [36]

$$1 \gtrsim \frac{\max_s |\langle E_i(s) | \partial_t H(t) | E_0(s) \rangle|}{|E_i - E_0|^2}, \text{ for all } i \neq 0. \quad (6)$$

A more rigorous statement can be found in Reference [37]. These theoretical guarantees assume a perfect annealing machine, isolated from any environment interference. By contrast, real machines are subject to noise, which increases the probability of the system escaping the ground state. They should be considered heuristic solvers, requiring empirical performance analysis [38].

### IV. PROBLEM HAMILTONIAN

Let  $Y$  be a disease  $Y$  and  $D = \{X_1, X_2, \dots, X_n\}$  a set of  $n$  candidate drugs. We propose as problem Hamiltonian

$$H_Y = \sum_{i=1}^n (z(Y, X_i) + \beta) S_i - \gamma \sum_{i < j} s(X_i, X_j) S_i S_j. \quad (7)$$

Here,  $S_i \in \{0, 1\}$  is a binary operator indicating the inclusion ( $S_i = 1$ ) or exclusion ( $S_i = 0$ ) of drug  $X_i$ , identical to the usual Ising spin Hamiltonian via the transformation  $S_i = (\mathbb{1} + \sigma_i^z)/2$ . This allows us to encode individual drug efficacy, quantified by the normalised z-score and categorise pairwise interactions between drugs as synergistic or antagonistic through the quadratic term  $s(X_i, X_j)$ . The hyperparameter  $\beta$  acts as a bias towards combinations of a smaller number of drugs (which are preferred in most scenarios), while  $\gamma$  balances the relative weight of pairwise interactions.

Clinical feasibility and computational practicality often necessitate limiting the number of drugs in a combination. It is possible to enforce the selection of exactly  $k$  drugs by appending a quadratic penalty term like

$$H_{\text{constraint}} = \lambda \left( \sum_{i=1}^n S_i - k \right)^2. \quad (8)$$

A high value for  $\lambda$  ensures the ground state satisfies  $\sum_i S_i = k$ . For instance, fixing  $k = 2$  restricts solutions to dual-drug therapies, which dominate clinical practice due to their reduced risk of adverse interactions and more manageable testing [5]. By introducing auxiliary variables, it is also possible to enforce multiple allowed combination sizes. In the special case where the two allowed sizes are consecutive integers, no ancilla are required and one can use the simpler term

$$H_{\text{constraint}} = \lambda \left( \sum_{i=1}^n S_i - k_1 \right) \left( \sum_{i=1}^n S_i - k_2 \right), \quad (9)$$

which penalizes all solutions except those with  $k_1$  or  $k_2$  drugs as long as  $|k_1 - k_2| \leq 1$ .

## V. HYPERPARAMETER CALIBRATION AND BENCHMARKING

We now describe the procedure used throughout this work to identify promising drug combinations using the problem Hamiltonian formalism. We subsequently apply this methodology to various diseases (see Section VII for results).

In order to choose a suitable pair of hyperparameters  $(\gamma, \beta)$  for the problem Hamiltonian (7) of a particular disease, a dataset consisting of validated drug combinations for various diseases was assembled. This constructed benchmarking dataset was obtained by filtering known effective drug combinations to retain only those whose individual constituents have documented disease associations. Further details, including data sources and preprocessing steps, are discussed in Appendix A. The resulting dataset, denoted by  $\mathcal{C}$ , serves as a reference to evaluate the performance of different hyperparameter choices in prioritizing known effective drug combinations. From the approved drug combinations in  $\mathcal{C}$ , we build a candidate drug set  $D$  by extracting unique drugs that

appear in at least one combination in  $\mathcal{C}$ . Comparing with the interactome data, we can determine the couplings  $z(Y, X_i)$  and  $s(X_i, X_j)$  for all  $X_i, X_j \in D$  (here  $Y$  refers to the chosen disease to be analysed). Then, for any pair  $(\gamma, \beta)$ , we can evaluate the spectrum of the problem Hamiltonian. As  $D$  is relatively small, it is feasible to enumerate all  $2^{|D|}$  configurations exactly, and rank them by their energy.

We evaluate the goodness of fit for a given pair  $(\gamma, \beta)$  with an average precision (AP) metric. AP is particularly suitable here, as it measures the concentration of validated combinations among the lowest-energy states and handles imbalanced datasets effectively. In more detail, let  $c_i$  be the  $i$ -th configuration in the energy ranking (with  $i = 1$  corresponding to the lowest energy configuration), and define a binary label  $y_i$  as

$$y_i = \begin{cases} 1, & c_i \in \mathcal{C} \\ 0, & \text{otherwise.} \end{cases}$$

We say that the precision at rank  $k$  is

$$P(k) = \frac{1}{k} \sum_{i=1}^k y_i, \quad (10)$$

and define the average precision of the spectrum as

$$\text{AP} = \frac{1}{|\mathcal{C}|} \sum_{k=1}^{2^{|D|}} P(k) y_k. \quad (11)$$

By construction,  $\text{AP} \in [0, 1]$ , with larger values indicating better prioritization of validated combinations among the lowest energy solutions.

Performing a grid search over the hyperparameter space we can find the optimal values  $(\gamma^*, \beta^*)$  for the chosen disease  $Y$  that maximize this metric. In our simulations, we selected a penalty term with  $\lambda_{\text{penalty}} = 10 \cdot \max(|z|, |\gamma \cdot s|)$  and incorporated a constraint of the form of Eq. (9) with  $k_1 = 2$  and  $k_2 = 3$ . This strongly favours combinations of size 2 and 3, which make up the bulk of the validated combinations dataset for all diseases in  $\mathcal{C}$ . Having selected the hyperparameters, we seek to apply our model to a larger candidate drug set  $\mathcal{D}$ , containing drugs that have not been validated in any combined therapy. This enlarged set is constructed by padding the original pool with randomly selected additional drugs, while ensuring that no strongly overlapping drugs lacking validated combination information are included. The size of this resulting set  $|\mathcal{D}|$  needs to be chosen to match the practical embedding and sampling limits of the available hardware, ensuring that the optimisation remains technically viable. By enlarging  $\mathcal{D}$ , we are populating the low-energy landscape to admit both known effective combinations and novel candidates whose network proximities to other drugs and the disease module resemble those of validated therapies. Thus, applying the learned hyperparameters  $(\gamma^*, \beta^*)$  to the

QUBO constructed for the expanded candidate set  $\mathcal{D}$  allows us to identify potential new drug combinations, including those involving previously untested drugs. We demonstrate how one can extract such predictions in the next section.

## VI. DRUG COMBINATION PREDICTION

In an ideal adiabatic process, the annealer is expected to return only the ground state configuration. However, in practice, hardware limitations can prevent the adiabatic evolution condition (6) from being satisfied. Together with uncontrollable noise, this causes the device to produce a distribution spanning many low-energy states, rather than a single ground state.

This aligns well with our goal of extracting multiple candidate combinations. We can leverage the non-idealities of the annealing process to explore a variety of low-energy configurations and thereby obtain many near-optimal drug combinations, which can be ranked and prioritised for experimental validation. To reproduce this behaviour on the previously mentioned enlarged QUBO ( $\mathcal{D}$ ), we employ an SQA sampler, D-Wave's `PathIntegralAnnealingSampler` [39], to reproduce the marginal distribution over low-energy states produced by a physical annealer. We used an exponentially increasing annealing schedule designed to promote transitions from the driver Hamiltonian's ground state into low-lying excited states of the problem Hamiltonian, with the schedule parameters heuristically tuned to balance escape probability and concentration on the low-energy region. As a result, a considerable number of runs escape the ground state of the problem Hamiltonian and sample a variety of configurations with similar (low) energy, which is precisely the regime where near-optimal drug combinations lie.

Following this scheme, the sampler is run  $R$  independent times. Each possible combination  $c$  will have been observed  $n_c$  times with corresponding frequency  $f_c = n_c/R$ . We then require a sufficiently large number of runs  $R$  so that  $f_c > 0$  for the combinations in the region of interest. With the majority of the probability mass concentrated on low-energy states, we can filter the lowest energy (generally highest frequency) configurations, which were not part of the validated combinations dataset, to set as our model's predictions for potential novel drug combinations and rank them accordingly.

This produces a ranked list of plausible novel combinations whose network-based profiles resemble those of validated therapies. Taken together, this approach provides a practical mechanism for extracting multiple candidate combinations from the quantum annealing process, effectively leveraging the hardware's characteristics to our advantage.

**TABLE I:** Calibrated hyperparameters  $(\gamma^*, \beta^*)$  and corresponding Average Precision (AP) for each disease.

Disease	$\gamma^*$	$\beta^*$	AP
Diabetes Mellitus	2.74	13.39	0.670
Rheumatoid Arthritis	5.18	14.47	0.594
Asthma	1.46	3.79	0.600
Brain Neoplasms	4.60	34.38	0.528

## VII. RESULTS

We applied the Hamiltonian framework and hyperparameter calibration pipeline to the four diseases with the most documented validated combinations in the benchmark dataset  $\mathcal{C}$ . The results below follow the methodology described previously.

Firstly, for each disease, we constructed a set of candidates  $\mathcal{D}$  from the unique drugs that make up its validated drug combinations. For the diseases Diabetes Mellitus and Rheumatoid Arthritis, these candidate sets consisted of 10 unique drugs, while for Asthma and Brain Neoplasms 9 such drugs were considered.

Using the interactome data, for each disease  $Y$  and drug pair  $X_i, X_j \in \mathcal{D}$ , we computed the network measures  $z(Y, X_i)$  and  $s(X_i, X_j)$ , which were then used to construct test QUBOs for specific hyperparameter pairs. By sweeping the hyperparameters  $(\gamma, \beta)$  and computing the Average Precision (AP) for each pair, we were able to determine the hyperparameters which maximize this metric  $(\gamma^*, \beta^*)$ .

The calibrated hyperparameter pairs  $(\gamma^*, \beta^*)$  and their corresponding Average Precision (AP) values for each disease are given in Table I.

The AP landscapes in the neighborhoods of these optimal points are displayed in Figure 2, showing a visible bias towards the first quadrant of the  $(\gamma, \beta)$  plane. This is consistent with the Complementary Exposure principle and further validates our Hamiltonian formulation.

To better visualize the prioritization of the validated combinations at the calibrated point, we inspect the bottom of the QUBO energy spectrum. Figure 3 shows how the validated combinations populate the low-energy region. The most pronounced structure is found for Diabetes Mellitus, which is also the disease with the largest number of documented combinations in  $\mathcal{C}$ . The observed tight clustering of matched combinations corresponds to a high AP and suggests that the network-proximity and separation metrics capture salient features of efficacious combinations. Conversely, higher dispersion (and lower AP) is indicative of either sparse benchmark data or disease biology that is less amenable to pairwise topological description. Namely, in the case of Brain Neoplasms, which holds the lowest AP, only one of the combinations present in  $\mathcal{C}$  contains three drugs (the remainder being pairwise combinations). This imbalance

in combination sizes is reflected in a considerably higher  $\beta^*$  value, which in turn greatly expands the energy range of the respective QUBO. This increase in scale usually tightens the spectral gap and can hinder optimisation when considering high numbers of drugs. These observations reinforce the need for a well-curated benchmark dataset and directly inform how confidently calibrated parameters can be used to search larger candidate spaces, i.e., concentrated spectra imply more confidently that low-energy configurations are meaningful targets for drug discovery, while interleaved spectra could be less trustworthy, requiring more conservative interpretations and motivating additional data collection. A visual depiction of how the representativeness of matched combinations degrades as we move up in energy and rank is provided by the Precision-Recall curves in Figure 4. A Precision-Recall curve plots precision (the fraction of retrieved solutions that are validated) against recall (the fraction of all validated combinations that have been retrieved) as one moves down the ranked list. The number of ground-truth positives ranges from 11–18, a small number compared to the total number of configurations, which explains the jaggedness of the curves.

For discovery, the calibrated hyperparameters  $(\gamma^*, \beta^*)$  were applied to example enlarged candidate sets  $\mathcal{D}$  of size  $|\mathcal{D}| = 50$  (the previous ones plus 40 or 41 new random drugs). We ran the SQA Sampler for 1024 independent runs, a quantity commonly used in quantum annealing experiments. The results in Figure 5 exemplify different marginal distributions that can be obtained with *pseudo-adiabatic* evolutions. We observe that the produced empirical frequencies are spread across many low-energy states, some of which include previously untested drugs. Even for the enlarged QUBO, which admits on the order of  $10^{15}$  possible drug combinations, we observe validated matches among the lowest-energy configurations. This suggests the calibrated hyperparameters generalize to larger candidate sets and points to possible therapeutic relevance of similar energy combinations.

The resulting ranked candidate lists are prioritization hypotheses grounded in network topology and intended to guide experimental validation rather than to stand as absolute proofs or clinical recommendations.

## VIII. DISCUSSION

We have introduced a network-medicine informed quantum annealing pipeline that encodes the Complementary Exposure principle as a QUBO and uses low-energy configurations to prioritise candidate drug combinations. The results, obtained for four exemplar diseases — Diabetes Mellitus, Rheumatoid Arthritis, Asthma, and Brain Neoplasms, demonstrate that low-energy states of the constructed Hamiltonian are considerably populated with validated combinations, indicating that topological proxies such as network

proximity and separation carry useful information for combination discovery.

Because our algorithm is driven exclusively by graph descriptors, its outputs should be read as ranked hypotheses rather than mechanistic or clinical proof. A low QUBO energy mainly identifies candidate combinations with high network proximity to the disease module while maintaining minimal target overlap — a correlative signal, not direct evidence of effectiveness or safety. Additionally, the hyperparameters that balance the cardinality of the combinations ( $\beta$ ) and pairwise interactions ( $\gamma$ ) were calibrated against a constructed benchmark of validated combinations and found to vary reasonably across the four diseases analysed. This dependence highlights that the fitted values are contingent on the composition and representativity of the benchmarking set. Thus, with small or skewed datasets, the calibrated hyperparameters are more likely to reflect dataset-specific properties than in transferable, disease-agnostic settings.

Relatedly, the Complementary Exposure principle itself was originally formulated and validated in restricted biological contexts (notably hypertension and cancer) and for drug pairs only. There is no *a priori* guarantee that the same topological signature of complementarity will hold universally across the entire disease spectrum. Accordingly, extending and applying the principle to new disease areas should be performed with per-disease validation.

Furthermore, while our construction can be restricted to pairwise combinations, it can also be applied to candidate sets of an arbitrary number of drugs, subject only to the usual computational and data constraints of problem embedding and sampling. Likewise, the interpretation of the quadratic coupling parameter  $\gamma$  is flexible. While positive  $\gamma$  emphasises complementary and non-overlapping targeting, scenarios where  $\gamma$  takes negative values could be explored to prioritise antagonistic interactions by consequence of overlapping exposure. In addition, the annealing paradigm naturally returns a distribution over many low-energy configurations rather than a single optimum, which is a strength in discovery settings, allowing harvesting of multiple near-optimal combination hypotheses from an astronomically large space.

Taken together, the quantum-annealing formulation we propose does not replace biological experimentation, rather, it narrows the combinatorial search space to a manageable, ranked list of novel hypotheses that can be prioritised for experimental testing. When used in this way, the framework can speed up the early stages of combination discovery.

If embedded within a rigorous experimental validation loop and complemented by pharmacological modelling, this approach could contribute to accelerating the identification of biologically plausible drug combinations and help focus resources on the most promising hypotheses.

## Acknowledgements

The authors would like to thank Lorenzo Buffoni for useful discussions on quantum annealing.

## Funding

This work was supported by FCT - Fundação para a Ciência e Tecnologia through project UIDB/50008/2020, with the DOI identifier 10.54499/UIDB/50008/2020, through project QuNetMed 2022.05558.PTDC, with the DOI identifier 10.54499/2022.05558.PTDC.

## Author Contributions

B. C. conceived the original idea of using quantum annealing for drug combination discovery. D. R. and

D.M. developed the quantum annealing framework. D. R. prepared the datasets and performed the numerical simulations. All authors contributed to the writing and revision of the manuscript.

## Data and Code Availability

All code required to reproduce the analyses, figures and experiments in this work is publicly available at <https://github.com/dmrapp/Drug-Combinations-using-Quantum-Annealers>. The validated benchmark disease-drug-combination dataset compiled for this study is included in that repository. All other datasets used in the study (interactome, drug-targets and disease-gene associations) are publicly available and their original sources are listed and cited in Appendix A.

---

[1] X. Sun, S. Vilar, and N. P. Tatonetti, *Science Translational Medicine* **5**, 205rv1 (2013), <https://www.science.org/doi/pdf/10.1126/scitranslmed.3006667>.

[2] V. Law *et al.*, *Nucleic Acids Research* **42**, D1091 (2013).

[3] A.-L. Barabási, N. Gulbahce, and J. Loscalzo, *Nature Reviews Genetics* **12**, 56 (2011).

[4] J. Menche, A. Sharma, M. Kitsak, S. D. Ghiaissian, M. Vidal, J. Loscalzo, and A.-L. Barabási, *Science* **347**, 1257601 (2015), <https://www.science.org/doi/pdf/10.1126/science.1257601>.

[5] F. Cheng, I. A. Kovács, and A.-L. Barabási, *Nature Communications* **10**, 1197 (2019).

[6] H. R. Grimsley, S. E. Economou, E. Barnes, and N. J. Mayhall, *Nature Communications* **10**, 3007 (2019).

[7] D. Niraula, J. Jamaluddin, M. M. Matuszak, R. K. T. Haken, and I. E. Naqa, *Sci Rep* **11**, 23545 (2021).

[8] J. a. P. Moutinho, A. Melo, B. Coutinho, I. A. Kovács, and Y. Omar, *Phys. Rev. A* **107**, 032605 (2023).

[9] J. P. Moutinho, D. Magano, and B. Coutinho, *Scientific Reports* **14**, 1026 (2024).

[10] D. Magano, J. Moutinho, and B. Coutinho, *SciPost Phys. Core* **6**, 058 (2023).

[11] P. Marques, A. Wichert, D. Magano, and B. Coutinho, *Quantum network-based prediction of cancer driver genes* (2025), arXiv:2510.12628 [quant-ph].

[12] E. Farhi, J. Goldstone, S. Gutmann, and M. Sipser, *Quantum computation by adiabatic evolution* (2000), arXiv:quant-ph/0001106 [quant-ph].

[13] T. Albash and D. A. Lidar, *Rev. Mod. Phys.* **90**, 015002 (2018).

[14] A. Das and B. K. Chakrabarti, *Rev. Mod. Phys.* **80**, 1061 (2008).

[15] A. D. King, A. Nocera, M. M. Rams, J. Dziarmaga, and et al., *Science* **388**, 199 (2025), <https://www.science.org/doi/pdf/10.1126/science.ado6285>.

[16] S. Kim, S.-W. Ahn, I.-S. Suh, A. W. Dowling, E. Lee, and T. Luo, *npj Quantum Information* **11**, 77 (2025).

[17] H. Salloum, R. Lukin, and M. Mazzara, *Quantum computing in drug discovery: A review of quantum annealing and gate-based approaches* (2024).

[18] A. Lucas, *Frontiers in Physics* **2**, 5 (2014).

[19] L. F. Pérez Armas, S. Creemers, and S. Deleplanque, *Scientific Reports* **14**, 16784 (2024).

[20] W. Sakuler, J. M. Oberreuter, R. Aiolfi, L. Asproni, B. Roman, and J. Schiefer, *Quantum Machine Intelligence* **7**, 43 (2025).

[21] E. Aguilera, J. de Jong, F. Phillipson, S. Taamallah, and M. Vos, *Mathematics* **12**, 10.3390/math12091291 (2024).

[22] J. Blenninger, D. Bucher, G. Cortiana, *et al.*, *Künstliche Intelligenz* **38**, 339 (2024).

[23] K. Kitai, J. Guo, S. Ju, S. Tanaka, K. Tsuda, J. Shiomi, and R. Tamura, *Phys. Rev. Res.* **2**, 013319 (2020).

[24] A. Perdomo-Ortiz, N. Dickson, M. Drew-Brook, G. Rose, and A. Aspuru-Guzik, *Scientific Reports* **2**, 571 (2012).

[25] Y. Li, X. Cui, Z. Xiong, Z. Zou, B. Liu, B.-Y. Wang, R. Shu, H. Zhu, N. Qiao, and M.-H. Yung, *Journal of Molecular Modeling* **30**, 228 (2024).

[26] A. Tučs, F. Berenger, A. Yumoto, R. Tamura, T. Uzawa, and K. Tsuda, *ACS Medicinal Chemistry Letters* **14**, 577 (2023).

[27] L. Meuser, A. Patsilinakos, and P. Faccioli, *Journal of Chemical Theory and Computation* **21**, 9993 (2025).

[28] A. Irbäck, L. Knuthson, S. Mohanty, and C. Peterson, *Phys. Rev. Res.* **6**, 013162 (2024).

[29] Y. Li, X. Cui, Z. Xiong, B. Liu, B.-Y. Wang, R. Shu, N. Qiao, and M.-H. Yung, *Journal of Chemical Theory and Computation* **20**, 6687 (2024).

[30] E. Güney, J. Menche, M. Vidal, and A.-L. Barabási, *Nature Communications* **7**, 10331 (2016).

[31] J. Menche, A. Sharma, M. Kitsak, S. D. Ghiaissian, M. Vidal, J. Loscalzo, and A.-L. Barabási, *Science* **347**, 1257601 (2015).

[32] A. Azad, S. Fatima, A. Capraro, S. A. Waters, and F. Vafaei, *Patterns* **2**, 100325 (2021).

- [33] E. L. Cao, *Frontiers in Natural Products* **2**, 1309994 (2024).
- [34] M. Iida, Y. Kuniki, K. Yagi, *et al.*, *Communications Medicine* **4**, 154 (2024).
- [35] T. Kadokawa and H. Nishimori, *Phys. Rev. E* **58**, 5355 (1998).
- [36] M. H. S. Amin, *Phys. Rev. Lett.* **102**, 220401 (2009).
- [37] A. Ambainis and O. Regev, An elementary proof of the quantum adiabatic theorem (2004), quant-ph/0411152.
- [38] J. King, S. Yarkoni, J. Raymond, I. Ozfidan, A. D. King, M. M. Nevisi, J. P. Hilton, and C. C. McGeoch, *Journal of the Physical Society of Japan* **88**, 061007 (2019), <https://doi.org/10.7566/JPSJ.88.061007>.
- [39] D-Wave Systems, Pathintegralannealsampler — d-wave ocean sampler, [https://docs.dwavequantum.com/en/latest/ocean/api\\_ref\\_samplers/index.html#dwave.samplers.PathIntegralAnnealingSampler](https://docs.dwavequantum.com/en/latest/ocean/api_ref_samplers/index.html#dwave.samplers.PathIntegralAnnealingSampler) (2021), accessed: 2025-10-15.
- [40] T. Rolland *et al.*, *Cell* **159**, 1212 (2014).
- [41] Rual, Jean-François, *et al.*, *Nature* **437**, 1173 (2005).
- [42] F. Zhu *et al.*, *Nucleic Acids Research* **40**, D1128 (2012).
- [43] T. Hernandez-Boussard *et al.*, *Nucleic Acids Research* **36**, D913 (2008).
- [44] A. Gaulton *et al.*, *Nucleic Acids Research* **40**, D1100 (2012).
- [45] T. Liu, Y. Lin, X. Wen, R. N. Jorissen, and M. K. Gilson, *Nucleic Acids Research* **35**, D198 (2007).
- [46] A. J. Pawson *et al.*, *Nucleic Acids Research* **42**, D1098 (2014).
- [47] UniProt Consortium, *Nucleic Acids Research* **47**, D506 (2019).
- [48] M. Zitnik, R. Sosić, S. Maheshwari, and J. Leskovec, BioSNAP Datasets: Stanford biomedical network dataset collection, <http://snap.stanford.edu/biodata> (2018).
- [49] G. Shtar, L. Azulay, O. Nizri, and et al., *Scientific Data* **9**, 263 (2022).

## Appendix A: Datasets

We have used the **human protein-protein interactome** compiled by Cheng, Kovács & Barabási (Nat Commun, 2019) [5] available in Supplementary Data 1, which

contains 243,603 protein-protein interactions connecting 16,677 proteins. The interactome was mapped to official gene symbols and Entrez IDs as described by Cheng *et al.* using GeneCards. The original data was collected from Rolland *et al.* [40] and Rual *et al.* [41], and from an unpublished CCSB dataset.

The **Drug-target interactions** were taken from Cheng, Kovács & Barabási (Supplementary Data 2), which aggregates DrugBank, the Therapeutic Target Database (TTD), PharmGKB, ChEMBL, BindingDB and the IUPHAR/BPS Guide to PHARMACOLOGY [2, 5, 42–46] and reviewed in the UniProt database [47].

More details on data preprocessing and filtering can be found under the Method section in Reference [5].

**Disease-gene associations** were obtained from the BioSNAP 'DG-AssocMiner' dataset (Stanford SNAP Biomedical Network Dataset Collection) [48], downloaded from <https://snap.stanford.edu/biodata/datasets/10012/10012-DG-AssocMiner.html> on 4 October 2024. The dataset contains 21,357 associations from 519 diseases to 7,294 gene nodes.

The disease-specific validated **Drug Combinations** dataset was constructed by intersecting the multi-drug combinations reported in the Continuous Drug Combination Database (CDCB) [49] with drug-disease associations compiled by Guney *et al.* [30]. A disease-combination pair was retained only if (i) the combination appears in CDCB as a verified multi-drug combination, and (ii) every drug in that combination is associated with the disease in Guney *et al.* — i.e., we required exact agreement between the set of drugs in the combination and the set of drugs associated with the disease. Applying this overlap and selection rule yields disease-combination pairs spanning 35 distinct diseases with at least one combination, 136 unique drugs, and 287 unique disease-combination pairs, 234 of which are constituted by two drugs, 40 are combinations of three drugs, and 13 of four or more drugs. The resulting dataset is publicly available in the associated project repository: <https://github.com/dmrapk/Drug-Combinations-using-Quantum-Annealers>.

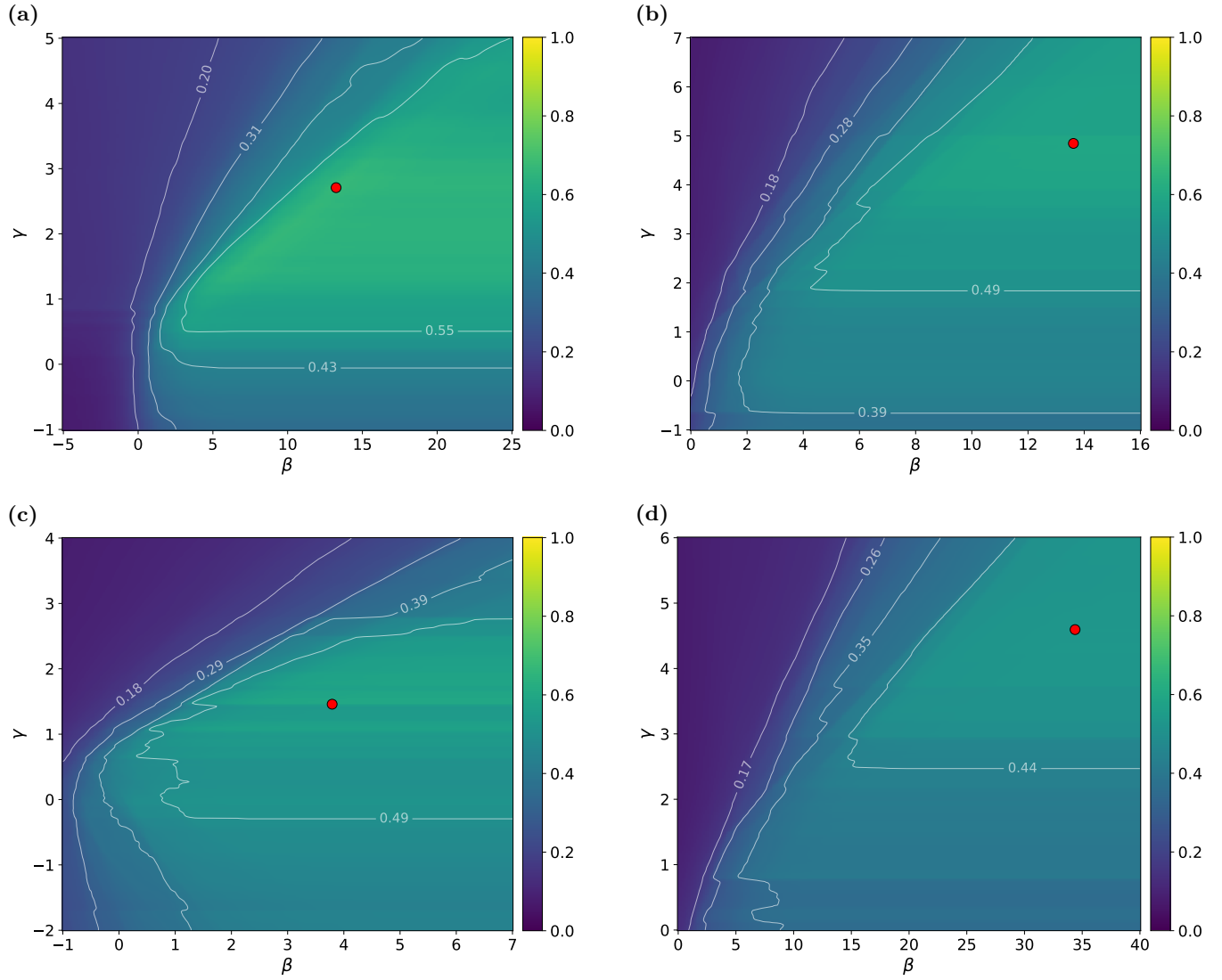


**Fig. 2: Average Precision (AP) Landscape.** Each subplot displays the AP values over a grid of hyperparameters ( $\gamma, \beta$ ) for the different diseases: (a) Diabetes Mellitus, (b) Rheumatoid Arthritis, (c) Asthma, and (d) Brain Neoplasms. The red dot in each plot indicates the optimal hyperparameter pair  $(\gamma^*, \beta^*)$  that maximizes the AP metric, reflecting the best prioritization of validated drug combinations among low-energy configurations.

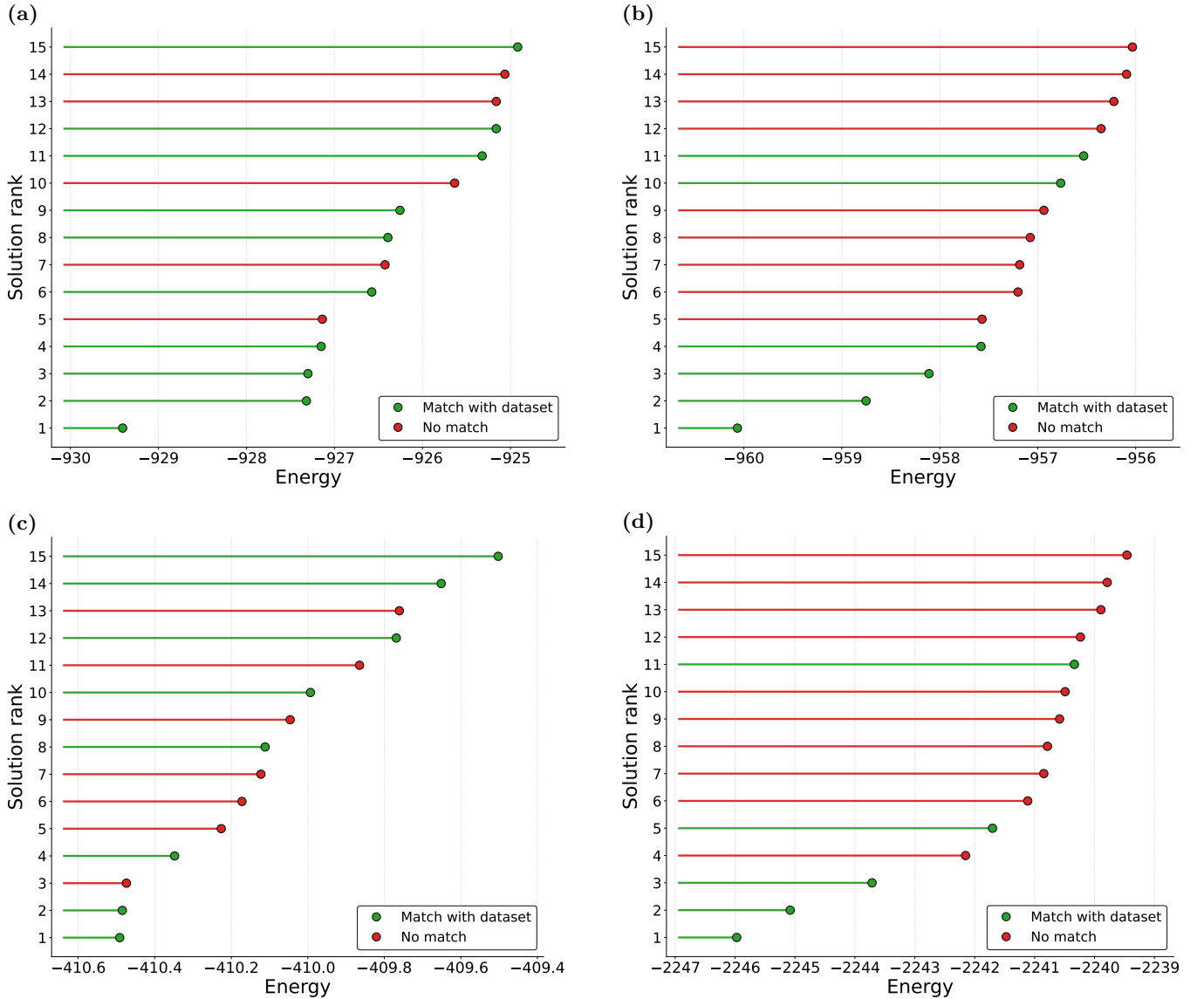


**Fig. 3: Energy spectrum at the optimal hyperparameters** Each subplot displays the top 15 lowest-energy configurations of the QUBO constructed from the initial candidate drug set at the disease-specific optimal hyperparameters  $(\gamma^*, \beta^*)$ . Solutions are ordered by increasing QUBO energy (lowest at the bottom) and are colour-coded to indicate whether the configuration matches a validated combination in the reference set  $\mathcal{C}$  or not. The diseases represented are: (a) Diabetes Mellitus, (b) Rheumatoid Arthritis, (c) Asthma, and (d) Brain Neoplasms.

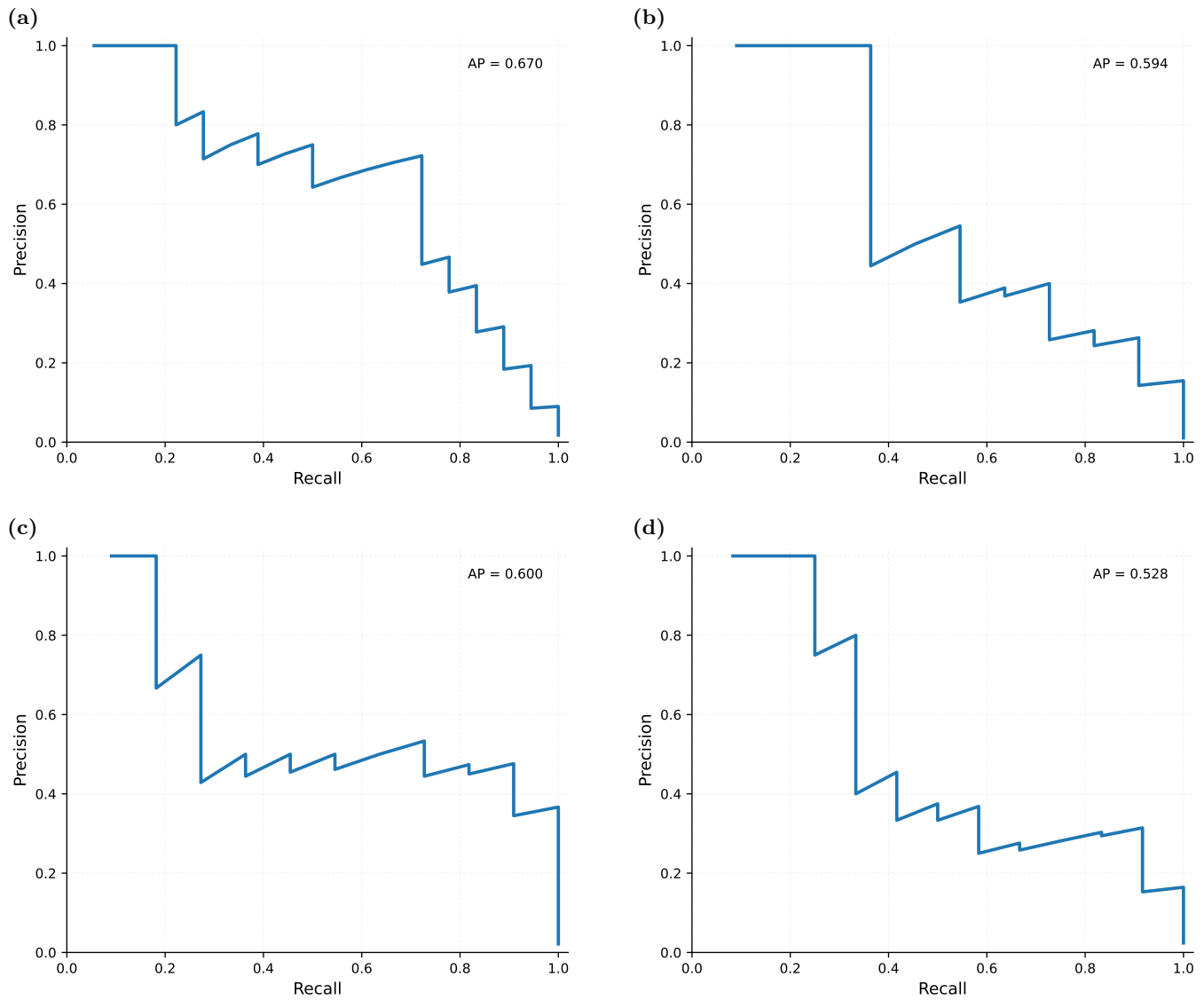


**Fig. 4: Precision-Recall Curve at the optimal hyperparameters.** Each subplot displays the Precision-Recall curve obtained by sweeping the ranked solutions of the QUBO constructed from the initial candidate drug set at the disease-specific optimal hyperparameters  $(\gamma^*, \beta^*)$ . The area under each curve corresponds to the Average Precision (AP) and quantifies the prioritization of validated drug combinations among the low-energy configurations. The diseases represented are: (a) Diabetes Mellitus, (b) Rheumatoid Arthritis, (c) Asthma, and (d) Brain Neoplasms.

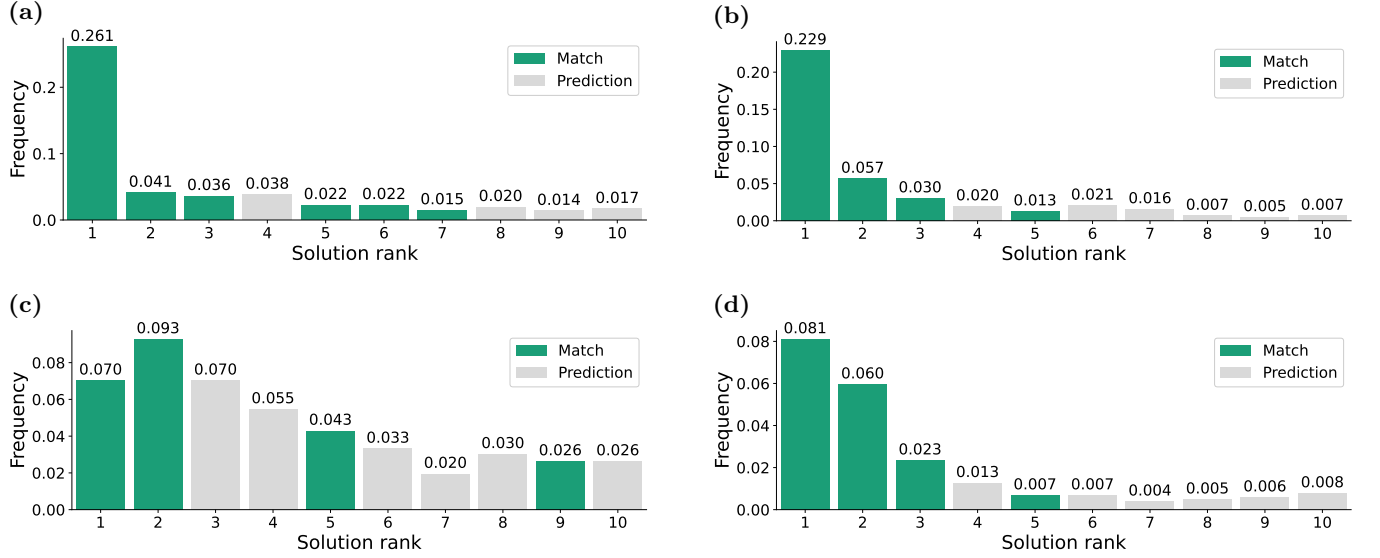


**Fig. 5: Sampled Simulated Quantum Annealing.** Each subplot displays the empirical frequency distribution from 1024 runs over the 10 lowest QUBO energies obtained by running the SQA sampler on the enlarged candidate drug set  $\mathcal{D}$  at the disease-specific optimal hyperparameters  $(\gamma^*, \beta^*)$ . Green markers indicate combinations found in  $\mathcal{C}$  while the remaining configurations are taken as predicted candidate synergistic combinations. The diseases represented are: (a) Diabetes Mellitus, (b) Rheumatoid Arthritis, (c) Asthma, and (d) Brain Neoplasms.